Localized Green Fabrication of Hydroxyapatite/ZnO Nanocomposite: Toward A Sustainable Antibacterial Biomaterial

Arie Hardian[1,2,*], Farah Nur Fauziyah[3], Teguh Karya[1], Dani Gustaman Syarif[4], Atiek Rostika Noviyanti[5], Jasmansyah[1], Muhammad Reza[6], Anceu Murniati[1,2], Kiki Adi Kurnia[7], Yanuar Setiadi[4], Ismunandar[8]

[1]Study Program of Master of Chemistry, Faculty of Sciences and Informatics, Universitas Jenderal Achmad Yani, Cimahi, West Java, Indonesia
[2]Material and Environmental Development Center, Universitas Jenderal Achmad Yani, Cimahi, West Java, Indonesia
[3]Department of Chemistry, Faculty of Sciences and Informatics, Universitas Jenderal Achmad Yani, Cimahi, West Java, Indonesia
[4]National Research and Innovation Agency (BRIN), Jalan Tamansari 71, Bandung 40132, Indonesia
[5]Department of Chemistry, Faculty of Mathematics and Natural Sciences, Universitas Padjadjaran, Sumedang, West Java 45360, Indonesia
[6]Department of Chemistry, Faculty of Mathematics and Natural Sciences, Universitas Jember, Jember, East Java 68121, Indonesia
[7]Postgraduate program of Science in Sustainability, Faculty of Infrastructure Planning, Universitas PERTAMINA, Jalan Teuku Nyak Arif, Jakarta 12220, Indonesia
[8]Division of Inorganic and Physical Chemistry, Institut Teknologi Bandung, Jalan Ganesha No. 10, Bandung 40132, Indonesia
*E-mail: arie.hardian@lecture.unjani.ac.id

Abstract. Using a plant-assisted sol–gel strategy, a hydroxyapatite–zinc oxide (HAp/ZnO) composite was produced from Padalarang calcite and lemon (Citrus limon L.) extract. The calcite supplied the calcium component, while constituents of the lemon extract promoted metal-ion complexation and helped control precursor stabilization. This environmentally friendly approach reduces the use of hazardous chemicals while facilitating the formation and stabilization of the composite precursor during the sol–gel process. The synthesized HAp/ZnO nanocomposite exhibited crystalline HAp and ZnO phases and the mean crystallite dimension calculated from the diffraction data was 45.52 nm. XRF analysis confirmed the elemental composition and Ca/P ratio, while FTIR spectroscopy

Received April 26th, 2026, Revised June 11th, 2026, Accepted for publication June 25th, 2026
 ISSN: 2337-5760, DOI: 10.5614/j.math.fund.sci.2025.58.1.1

identified the characteristic functional groups of HAp and ZnO. Further, SEM observations revealed the particle morphology of the nanocomposite. In disk-diffusion testing against *Escherichia coli*, the inhibition diameter increased from 5 mm at 5 mg/mL to 15 mm at 20 mg/mL. The antibacterial response was interpreted mainly in terms of ZnO-derived reactive oxygen species and the action of released Zn^{2+} ions. The findings of this study indicate that the synthesized HAp/ZnO nanocomposite is a promising candidate material for further investigation in the development of sustainable antibacterial biomaterials.

Keywords: *antibacterial performance; environmentally benign synthesis; hydroxyapatite; Padalarang calcite; sustainable biomaterial; zinc oxide nanoparticles.*

1 Introduction

Hydroxyapatite (HAp), $Ca_{10}(PO_4)_6(OH)_2$, has received extensive attention as a biomaterial because its chemical and structural resemblance to the mineral component of bone provides favorable biocompatibility. This similarity underlies its generally favorable biocompatibility and explains its use in bone substitutes, dental implants, and orthopedic surface layers [1,2]. Nevertheless, unmodified HAp is mechanically brittle and does not inherently provide sufficient antibacterial protection, which can limit its performance in implant-related environments where infection control is essential [3]. Consequently, composite design has been widely used to improve HAp performance while introducing antimicrobial functionality.

One common strategy is to combine HAp with antibacterial metal oxides, particularly zinc oxide (ZnO), because ZnO is biologically compatible and active against a broad range of microorganisms. Sinulingga et al. [4] showed that metal-ion-modified HAp exhibited stronger antibacterial behavior than undoped HAp. ZnO is especially attractive, because it can act against both Gram-positive and Gram-negative microorganisms [5]. Its antibacterial action has been associated with membrane damage, reactive oxygen species (ROS) generation, and disruption of microbial metabolic processes [6,7]. Incorporating ZnO into an HAp matrix may therefore preserve the biocompatible character of HAp while providing additional antibacterial performance for biomedical applications.

The identity of the calcium precursor strongly affects the purity and properties of the resulting HAp. Calcite-rich limestone, which contains approximately 40.04% calcium, offers an inexpensive and abundant feedstock for calcium-based materials [4]. Indonesia has extensive limestone resources and Padalarang in

West Java is recognized as a source of high-purity calcite that can be converted into a suitable precursor for HAp production [8]. Using this local mineral can reduce raw-material costs and support the development of more regionally sustainable biomaterials.

The processing route also determines the final structure and performance of HAp/ZnO materials. Traditional chemical syntheses may involve corrosive reagents, toxic auxiliaries, or energy-intensive treatment, which creates safety and environmental burdens. Plant-assisted synthesis offers a lower-impact alternative because natural extracts can act as complexing, surface-capping, and stabilization media. Their metabolites—including organic acids, flavonoids, and alkaloids—can influence nucleation and particle growth [9,10]. In the present work, lemon (*Citrus limon* L.) extract was selected because its citric acid and related organic constituents can interact with metal ions and particle surfaces during sol-gel formation. Citric acid may coordinate Ca and Zn species, while its carboxyl groups can help stabilize the developing particles and limit agglomeration [11,12].

Green-synthesized HAp is sensitive to processing variables such as temperature, reaction time, and pH. Among these factors, solution pH strongly influences particle morphology. Highly alkaline conditions, for example near pH 9, tend to favor more spherical HAp particles. At moderately acidic conditions around pH 6, elongated nanorods or plate-like structures may be favored, whereas more acidic media near pH 4 can lead to complex three-dimensional morphologies such as microfibers, microtubes, or feather-like structures [13].

Although HAp has been investigated extensively for biomedical use, fewer studies have focused on preparing it from Padalarang calcite. The combined use of Indonesian mineral resources and plant-assisted green processing for HAp/ZnO preparation also remains insufficiently explored. Addressing this gap could enable the production of functional biomaterials that are less costly, more environmentally responsible, and more closely linked to locally available resources.

To address this research gap, the present work produced an HAp/ZnO composite by combining locally obtained Padalarang calcite with lemon-extract-assisted sol–gel processing. XRF, XRD, FTIR, and FE-SEM were employed to determine elemental composition, phase constitution, crystallinity, functional groups, and

surface morphology. The antibacterial response against *Escherichia coli* was then examined as an initial indication of functional performance. By coupling a regional calcium resource with a plant-derived processing aid, the study explored a lower-cost and more sustainable route toward antibacterial mineral-based materials.

2 Experimental Section

2.1 Materials

Padalarang calcite, fresh lemon (Citrus limon L.), distilled water, sterile paper disks, and Whatman filter paper were used in the experiments. The chemical reagents were zinc nitrate tetrahydrate (Merck, analytical grade, 98%), sodium hydroxide (Merck, analytical grade, ≥99% on an NaOH basis), $(NH_4)_2HPO_4$ (Merck, ACS grade, ≥98%), and Tryptic Soy Agar supplied by Sigma-Aldrich.

2.2 Methods

The procedures were adapted from previously published green-synthesis and biomaterial-preparation methods, with modifications tailored to the present study. The principal changes were the use of Padalarang calcite as a local calcium precursor, lemon extract as a naturally derived complexing, capping, and stabilizing medium, and the incorporation of ZnO nanoparticles into the HAp phase under selected sol-gel and calcination conditions.

2.2.1 Preparation of Lemon Extract

Lemon juice was prepared with modifications to the protocol of Nakilcioğlu-Taş and Ötleş [14]. Fresh fruit was cleaned with distilled water, allowed to dry at ambient temperature, and manually pressed. The expressed liquid was vacuum filtered through Whatman paper to remove pulp and suspended material. It was subsequently centrifuged at 13,133 × g (10,000 rpm) for 6 min to reduce the remaining particulate impurities. The clarified extract was either used directly or stored at 4 °C for no more than 4 h [14].

2.2.2 Synthesis of ZnO Nanoparticles

ZnO was synthesized by adapting previously reported plant-assisted sol–gel procedures [12,15,16]. In the preparation used here, lemon extract functioned as the complexing and capping medium. Zinc nitrate tetrahydrate (2 g) was

introduced into 100 mL of a 6.25% (v/v) lemon-extract solution. After 1 h of stirring at ambient temperature, the mixture was heated to 60 °C and maintained under agitation at 600 rpm until a $Zn(OH)_2$-containing sol developed. Drying at 120 °C for 4 h produced a porous solid intermediate, which was converted to a fine white ZnO powder by calcination at 550 °C for 4 h. The extract content, mixing conditions, and thermal treatment were selected to generate ZnO suitable for incorporation into the HAp phase.

2.2.3 Synthesis of HAp/ZnO Nanocomposite

The HAp/ZnO composite was obtained by modifying sol–gel procedures previously used for calcium-rich natural precursors and HAp/ZnO systems [11,13,18].

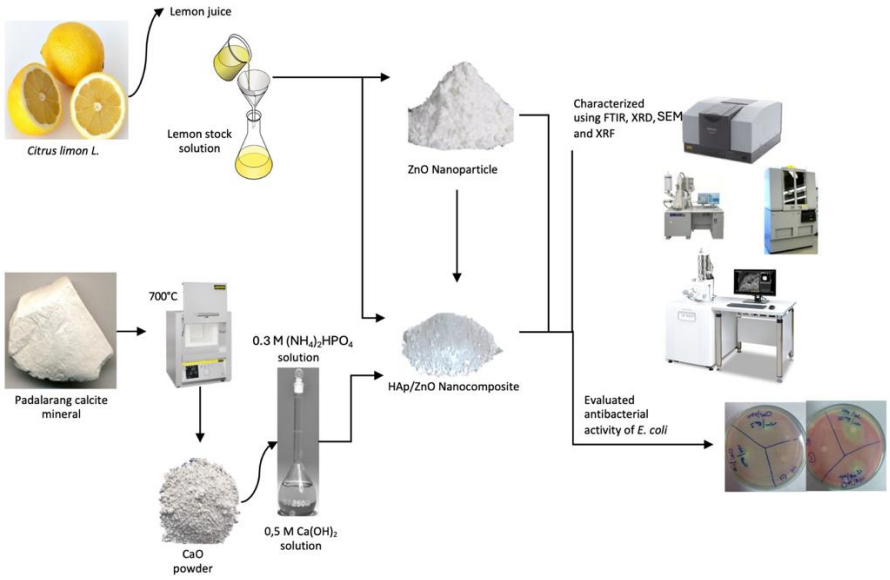

Figure 1 Schematic overview of the plant-assisted sol-gel preparation of HAp/ZnO using Padalarang calcite as the calcium precursor and lemon extract as the natural chelating, capping, and stabilizing agent.

Padalarang calcite was calcined at 700 °C for 4 h to convert $CaCO_3$ into CaO. A 2.8 g portion of the resulting CaO was dispersed in 100 mL of distilled water to form a 0.5 M $Ca(OH)_2$ suspension. Under continuous stirring, this calcium source was reacted with 0.3 M $(NH_4)_2HPO_4$ to generate the HAp precursor. Separately, 0.1017 g of ZnO was dispersed in 10 mL of distilled water and added to the

precursor mixture, giving a Ca:Zn molar ratio of 4:1. Lemon extract (10 mL) was then introduced gradually, and the pH was adjusted to 9 with 0.1 M NaOH. The mixture was maintained at 50 °C for 30 min and subsequently heated at 120 °C until gelation. The gel was dried at 80 °C for 12 h and calcined at 700 °C for 4 h to produce the final composite powder. The schematic of the synthesis is shown in **Fig. 1**.

2.2.4 Characterization Techniques

A combination of diffraction, spectroscopic, elemental, and microscopic methods was used to characterize the composite. XRD data were recorded with a Rigaku MiniFlex instrument using Cu Kα radiation (λ = 0.15406 nm) over 2θ = 10–80° with a step interval of 0.02°. Bulk elemental composition and the Ca/P ratio were determined by wavelength-dispersive XRF. FTIR spectra were collected with a Shimadzu IRPrestige-21 spectrometer between 4000 and 400 cm^{-1} using KBr pellets. Particle morphology and size distribution were examined with a Hitachi SU3500 scanning electron microscope, and elemental mapping was performed by energy-dispersive X-ray spectroscopy.

2.2.5 Antibacterial Activity Test

The antibacterial response toward *Escherichia coli* was investigated by a modified disk-diffusion assay. Sterilized TSA was poured into Petri dishes, after which an *E. coli* suspension of approximately 10^8 CFU/mL was spread uniformly across the agar. Sterile paper disks were loaded with HAp/ZnO suspensions containing 0, 5, 10, 15, or 20 mg/mL and positioned on the inoculated plates. Following incubation at 37 °C for 24 h, the diameter of each clear zone surrounding the disks was measured.

Each concentration was examined once as an initial screening experiment. Consequently, replicate-derived uncertainty, standard deviation, and statistical significance could not be reported, and the observations are presented descriptively. Activity was interpreted using the Davis and Stout scale: weak (<5 mm), moderate (5–10 mm), strong (10–20 mm), and very strong (≥20 mm).

3 Results And Discussion

3.1 ZnO Nanoparticle

The modified green sol-gel route yielded a fine white ZnO powder with lemon extract acting as the natural complexing and capping medium. During the process, citric acid and other organic constituents of the extract likely coordinated Zn^{2+} species before hydrolysis, condensation, gelation, and thermal conversion to ZnO. Carboxyl groups in citric acid can bind zinc-containing species and stabilize the precursor sol, which may suppress uncontrolled growth and reduce agglomeration. The overall process is therefore more appropriately interpreted as a sol-gel transformation involving complex formation, hydrolysis, condensation, and decomposition during calcination, as outlined in Figure 2.

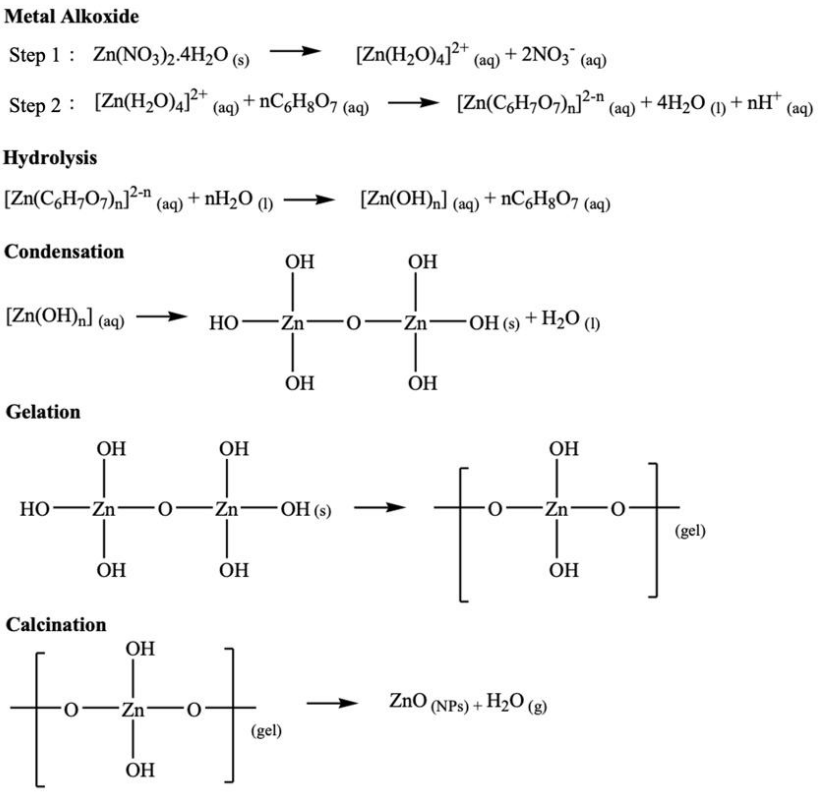

Figure 2 Proposed sequence of chemical transformations during the lemon-extract-assisted sol-gel preparation of ZnO nanoparticles.

3.2 HAp/ZnO Nanocomposite

The green sol-gel procedure produced a grayish-white HAp/ZnO composite powder. The HAp precursor was initially generated by reacting $Ca(OH)_2$ with $(NH_4)_2HPO_4$ through a conventional precipitation pathway. ZnO nanoparticles and lemon extract were then introduced as key components of the green processing route. Owing to its citric acid content, lemon extract likely complexed metal species and contributed to particle capping and stabilization. Carboxyl groups may interact with Ca^{2+}, ZnO surfaces, and HAp precursor particles, thereby improving dispersion, reducing particle agglomeration, and supporting composite formation. Adjustment to alkaline pH with NaOH may also have influenced species solubility and precursor stability. Subsequent drying and calcination at 700 °C removed water and most residual organic matter while promoting crystallization of the HAp/ZnO product. A proposed reaction scheme is shown in Figure 3.

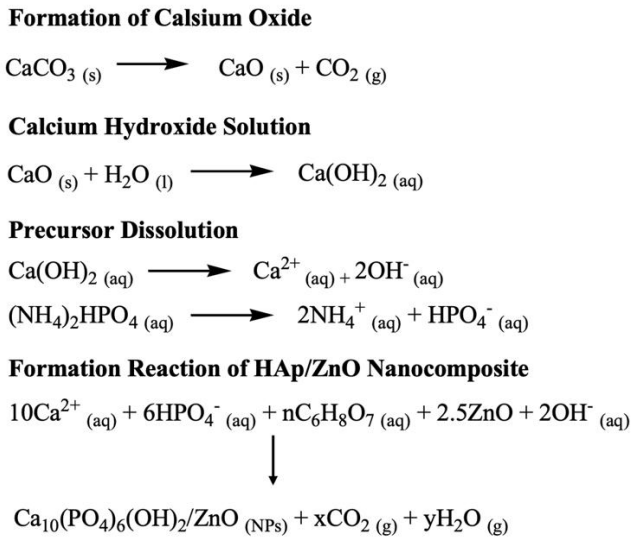

Figure 3 Proposed reaction pathway for forming the HAp/ZnO nanocomposite from calcite-derived calcium species, phosphate ions, ZnO, and lemon-extract constituents.

XRD was used to identify the crystalline phases and evaluate the structural features of the prepared composite. The measured diffractogram was compared

with reference patterns for HAp (ICSD 157481), ZnO (ICSD 157132), and tricalcium phosphate (TCP; ICSD 89320), as presented in Figure 4.

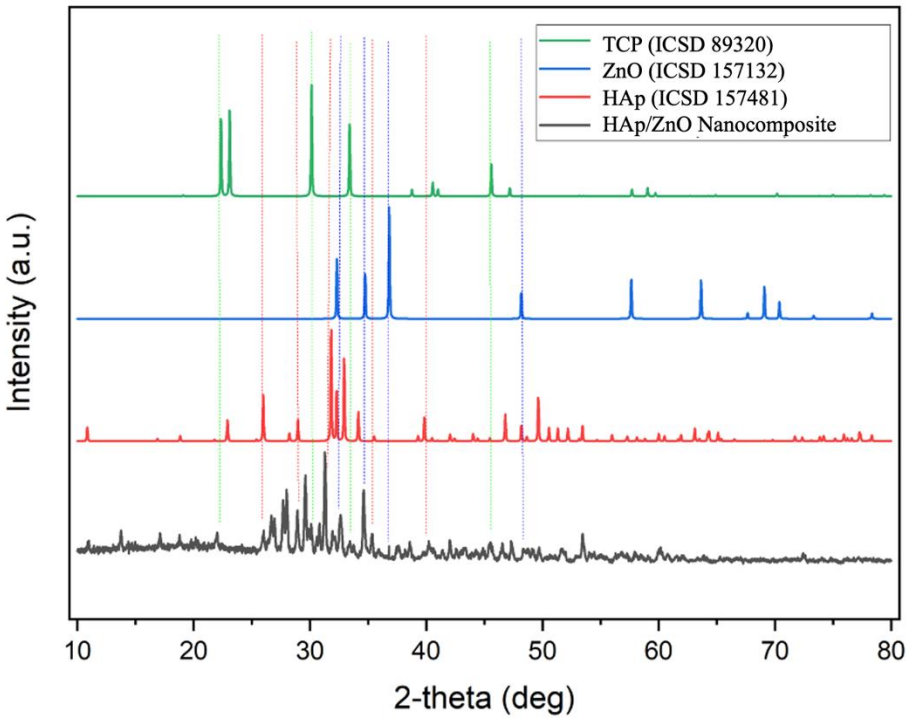

Figure 4 Experimental XRD pattern of the HAp/ZnO composite compared with reference reflections for HAp, ZnO, and TCP.

Several diffraction features characteristic of HAp were observed, particularly within the 2θ region of approximately 25°–35° [19]. The reflection near 31.28° is assignable to crystalline HAp and confirms formation of the hydroxyapatite phase [13]. ZnO was identified from reflections at about 32.25°, 34.62°, 36.80°, and 48.24°, which correspond to the ZnO reference pattern ICSD 157132 [16]. Additional low-intensity reflections around 22.17°, 30.18°, 33.47°, and 45.31° indicate that a small amount of TCP was also present as a secondary calcium-phosphate phase.

TCP formation may be related to carbonate incorporation and partial destabilization of HAp during calcination. Residual carbonate species originating from calcite can release CO_2 at elevated temperature, and carbonate may also substitute partly into the HAp lattice under moist conditions. Such substitution

can reduce the thermal stability of HAp and favor conversion to TCP. Literature reports indicate that TCP begins to develop near 700 °C, becomes increasingly crystalline as temperature rises, and remains stable at approximately 1200–1400 °C [17]. The Scherrer calculation yielded a mean crystallite size of 45.52 nm for the HAp/ZnO powder [18].

The Ca/P ratio measured by XRF was 1.57 (Table 1), whereas stoichiometric HAp has a theoretical value of 1.67. This difference implies that the product is not composed solely of stoichiometric hydroxyapatite and may contain calcium-deficient HAp and/or secondary calcium-phosphate phases. Lower Ca/P values are commonly linked to calcium-deficient apatite, which can partially transform into TCP during high-temperature treatment [15,16]. In the present system, calcination at 700 °C may have induced dehydroxylation and rearrangement of the apatite lattice, facilitating partial conversion of calcium-deficient HAp into TCP. This explanation agrees with the weak TCP reflections detected by XRD.

Table 1 Bulk elemental composition and Ca/P ratio of the HAp/ZnO composite determined by XRF.

Sample	Composition (%w/w)			Composition (%mol)		
	Ca	P	Zn	Ca	P	Zn
HAp/ZnO	61.8	30.2	6.88	1.54	0.98	0.11

The reduced Ca/P ratio may also reflect the presence of ZnO in the HAp matrix. During sol-gel processing, ZnO particles may interact with calcium-phosphate precursors and alter HAp nucleation and growth. Zinc-containing species could compete with Ca^{2+} at developing crystal surfaces or perturb the local arrangement of calcium and phosphate ions, thereby favoring non-stoichiometric apatite. Although FTIR evidence indicates that the material is mainly a physical composite rather than a newly bonded chemical phase, ZnO may still modify the local chemical environment, particle dispersion, and crystallization behavior of HAp.

FTIR analysis was conducted to determine the principal bonding environments in the composite. The spectrum contained the principal signals of hydroxyapatite, including OH^-, PO_4^{3-}, and CO_3^{2-} groups, together with a band attributable to Zn-O. Bands at approximately 560, 740, 960, and 1050 cm^{-1} were assigned to phosphate bending and stretching modes, whereas features near 2900 and 2061

cm^{-1} were associated with hydroxyl-related vibrations [15]. A broad OH absorption around 3000 cm^{-1} further supported the presence of HAp [11]. The band near 470 cm^{-1} was assigned to Zn-O stretching, confirming the inclusion of ZnO in the composite [16,17].

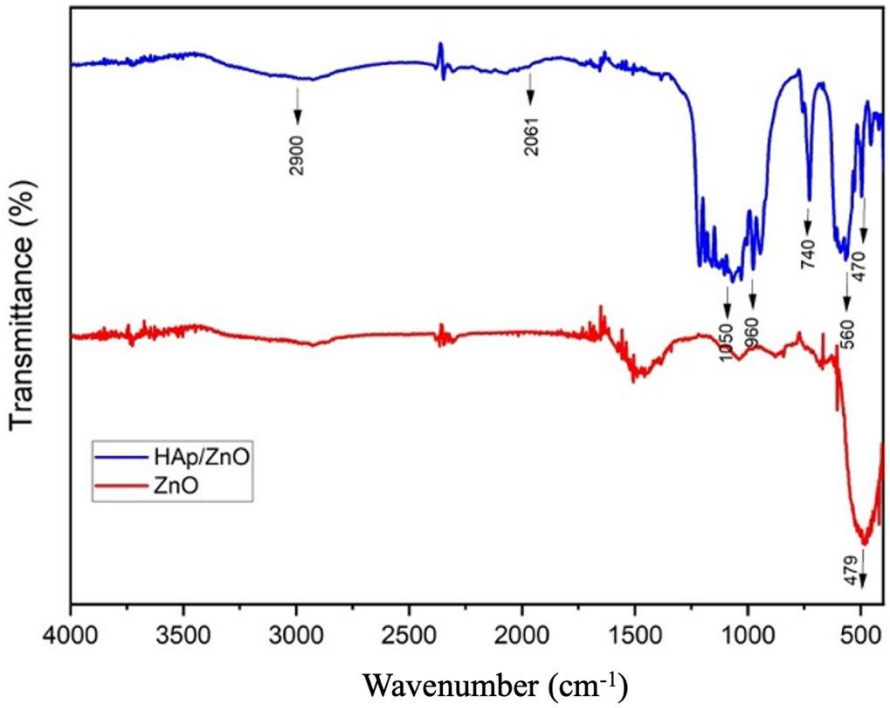

Figure 5 FTIR profiles of ZnO and the synthesized HAp/ZnO composite, showing the principal phosphate-, hydroxyl-, and Zn–O-related bands.

No additional absorption bands or pronounced shifts were detected after incorporating ZnO, suggesting that no new chemical bonds detectable by FTIR were generated. The composite is therefore considered to be formed predominantly through physical interactions. These interactions may include attachment of ZnO particles to HAp surfaces, weak electrostatic attraction, hydrogen-bond-like interactions involving surface hydroxyl groups, and interfacial contact between ZnO surface species and HAp sites such as PO_4^{3-}, OH^-, and Ca^{2+}. Figure 6 illustrates a possible model in which ZnO particles are distributed over HAp surfaces without forming new covalent or ionic bonds. This interpretation is consistent with the coexistence of crystalline HAp and ZnO in

the XRD pattern and with preservation of the characteristic functional groups of both components in the FTIR spectrum.

Based on this interpretation, a schematic illustration (Figure 6) of the possible physical interactions between HAp and ZnO is proposed. In this model, ZnO nanoparticles are distributed on the surface of the HAp matrix without forming new covalent or ionic bonds. This interpretation is consistent with the coexistence of crystalline HAp and ZnO in the XRD pattern and with preservation of the characteristic functional groups of both components in the FTIR spectrum.

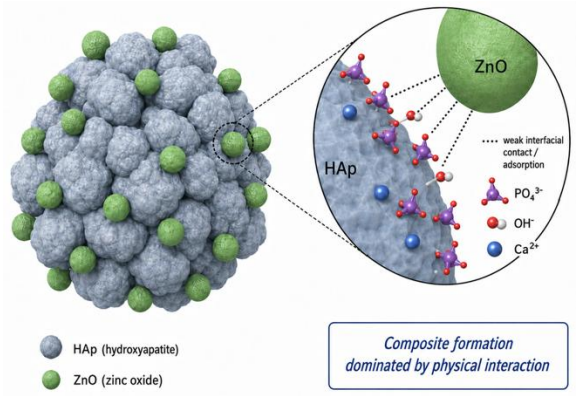

Figure 6 Conceptual representation of the predominantly physical interfacial interactions between HAp and ZnO in the composite.

FE-SEM was used to assess the external morphology of the composite. As shown in Figure 7a, the particles were irregular to nearly rounded and had apparent dimensions of about 143–157 nm. These values are considerably larger than the 45.52 nm crystallite size obtained from XRD, indicating that the objects visible by SEM are aggregates composed of several smaller coherent crystallites.

This difference is expected because XRD and SEM describe different structural scales. XRD-derived crystallite size corresponds to coherently diffracting crystalline domains, whereas SEM measures the external dimensions of individual particles or agglomerates. Therefore, the particles visible in SEM likely comprise multiple nanocrystalline domains joined into larger secondary structures. The combined results indicate a nanocrystalline HAp/ZnO material that forms larger aggregates observable by electron microscopy.

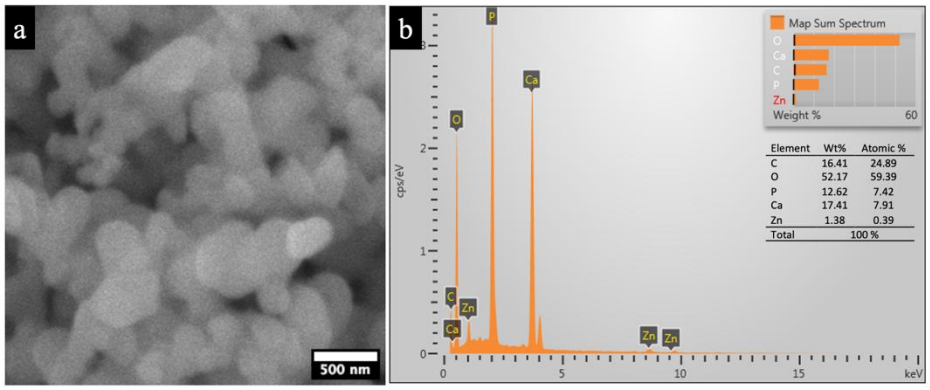

Figure 7 (a) FE-SEM image and (b) EDX spectrum of the synthesized HAp/ZnO composite.

Signals from Ca, O, P, and Zn were present in the EDX spectrum (Figure 7b), confirming that calcium-phosphate and zinc-containing components occurred in the analyzed region. Elemental mapping likewise indicated Zn-containing domains distributed within a calcium-phosphate matrix. The Ca/P molar ratio calculated from EDX was 1.07, below the bulk value of 1.57 determined by XRF. This difference may reflect near-surface phosphate enrichment or the different sampling depths and sensitivities of the two techniques.

The Ca/P value obtained by EDX was also below the ideal HAp ratio of 1.67, again indicating possible calcium-deficient apatite and/or TCP. This interpretation agrees with the weak TCP reflections in the XRD pattern. TCP formation during thermal treatment depends on multiple variables, including composition, crystal structure, morphology, dispersion, and other physicochemical features of the HAp precursor [19]. At elevated calcination temperatures, loss of hydroxyl groups from HAp can promote partial conversion to TCP [20]. The presence of TCP may be beneficial for some applications because TCP generally resorbs more readily through osteoclast-mediated processes than stoichiometric HAp [21].

The difference between the XRF and EDX Ca/P ratios reflects the distinct analytical volumes sampled. XRF represents the bulk elemental composition, whereas EDX is more sensitive to the near-surface region and to the specific micro-area selected for analysis. Thus, the lower EDX ratio may indicate localized phosphate-rich regions, heterogeneous ZnO distribution, or surface

formation of calcium-deficient phases. Overall, the data support a multiphase composite consisting primarily of HAp and ZnO, with a minor TCP contribution arising from non-stoichiometry and thermal treatment.

3.3 Antibacterial Activity of *Escherichia coli* Results

Disk-diffusion testing was used to examine the response of Gram-negative *E. coli* to the composite. This organism was selected because it grows rapidly and is commonly associated with the human intestinal tract [22]. HAp/ZnO suspensions containing 0, 5, 10, 15, and 20 mg/mL were evaluated. After 24 h at 37 °C, inhibition diameters were recorded and interpreted using the Davis and Stout categories: weak (<5 mm), moderate (5–10 mm), strong (10–20 mm), and very strong (≥20 mm).

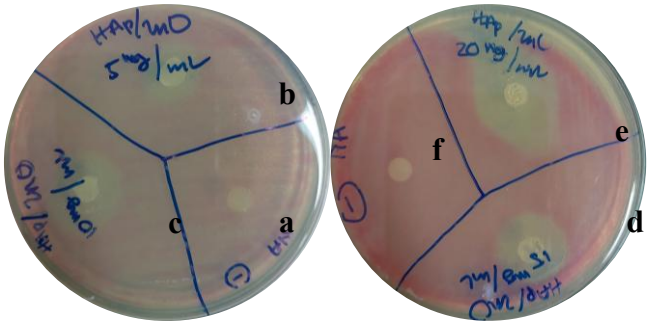

Figure 8 Disk-diffusion plates showing the response of *E. coli* to HAp/ZnO at 0, 5, 10, 15, and 20 mg/mL.

The data in Table 2 show that antibacterial performance increased with composite concentration. At 5 mg/mL, a 5 mm inhibition zone was observed, corresponding to moderate activity and demonstrating measurable antibacterial behavior even at the lowest non-zero concentration. Increasing the concentration to 20 mg/mL enlarged the inhibition zone to 15 mm, which falls within the strong category. El-Bassyouni et al. [23] reported inhibition zones of approximately 11–13 mm for a 50 mg ZnO-doped HAp specimen containing 5 wt% ZnO. Although the experimental conditions differ, both studies show that antibacterial performance depends on the amount of ZnO-containing material present.

Table 2 Inhibition-zone diameter and antibacterial classification of HAp/ZnO against *E. coli* at different composite concentrations.

HAp/ZnO Nanocomposites Concentration (mg/mL)	Inhibition Zone Diameter (mm)	Category
0	0	Weak
5	5	Moderate
10	8	Moderate
15	10	Strong
20	15	Strong

Because the composite underwent high-temperature calcination, most organic constituents from the lemon extract were expected to decompose and are unlikely to account directly for the observed antibacterial effect. The response is therefore attributed mainly to the ZnO fraction. This interpretation is consistent with earlier findings that HAp/ZnO systems inhibit Gram-negative bacteria such as *E. coli* more effectively than undoped HAp, which normally has limited intrinsic antibacterial activity [23].

The antibacterial action may involve oxidative stress generated at the ZnO surface. Redox processes or electronic excitation can produce reactive oxygen species that injure the bacterial envelope and impair membrane integrity [24]. Dissolved Zn^{2+} may provide an additional contribution by binding to imidazole, thiol, carboxylate, and amino functionalities in microbial proteins. These interactions can alter protein conformation, increase membrane permeability, interfere with cellular transport, and ultimately promote cell death [24].

The observed inhibition indicates that the synthesized HAp/ZnO material merits further study as an antibacterial biomaterial candidate. However, the present investigation was limited to physicochemical characterization and a preliminary single-run assay against *E. coli*. Biocompatibility, cytotoxicity, hemocompatibility, and in vivo safety were not examined. Potential use in bone-tissue engineering, wound healing, or antimicrobial implant coatings should therefore be treated as a future research direction rather than a demonstrated biomedical function.

Additional studies should investigate interactions with relevant mammalian cells, including osteoblast-like cells, fibroblasts, or stem cells depending on the

intended application. Cytotoxicity, adhesion and proliferation, inflammatory response, mechanical stability, and in vivo biocompatibility must be evaluated before biological safety and functional suitability can be established. The current results provide a preliminary foundation but are not sufficient to confirm direct clinical or biomedical applicability.

4 Conclusion

An HAp/ZnO composite was produced from Padalarang calcite and lemon extract through an extract-assisted sol–gel process. Diffraction and spectroscopic results showed that crystalline HAp and ZnO were present, together with a minor secondary calcium-phosphate contribution, and the calculated mean crystallite size was 45.52 nm. Microscopy and elemental analyses supported formation of a multiphase calcium-phosphate/ZnO material. Against *Escherichia coli*, the inhibition diameter increased with concentration, demonstrating a concentration-responsive antibacterial effect.

The ZnO component was the principal contributor to antibacterial behavior, supporting continued investigation of the composite as a candidate for antibacterial biomaterial development. The study did not assess biocompatibility, cytotoxicity, mechanical behavior, or in vivo biological safety. Accordingly, applications in bone regeneration, wound care, and antimicrobial coatings remain prospective rather than confirmed. Future work should include replicated antibacterial testing, mammalian-cell compatibility, cytotoxicity, mechanical evaluation, and in vivo response to determine whether the material is suitable for biomedical use.

Acknowledgements

Financial support was provided by the Ministry of Research, Technology, and Higher Education of the Republic of Indonesia (Kemdiktisaintek) under grants DRTPM 106/E5/PG.02.00/PL/2024, 016/SP2H/RT-MONO/LL4/2024, 004/SPK/LPPMUNJANI/VI/2024 for PPS-PTM, and 003/SPK/LPPMUNJANI/VI/2024 for PFR. Additional funding was received through the 2024 Universitas Jenderal Achmad Yani Research Grant program (SKEP/131/UNJANI/V/2024).

References

[1] Karunakaran, G., Cho, E.B., Kumar, G.S., Kolesnikov, E., Sudha, K.G., Mariyappan, K., et al., Citric Acid-Mediated Microwave-Hydrothermal Synthesis of Mesoporous F-Doped HAp Nanorods from Bio-Waste for Biocidal Implant Applications, *Nanomaterials*, **12**(315), pp. 1-19, 2022.

[2] Suparto, I.H. & Putri. D.K., Synthesis of Hydroxyapatite from Rice Fields Snail Shell (*Bellamya javanica*) through Wet Method and Pore Modification Using Chitosan, *Procedia Chem.*, **17**, pp.27-35, 2015.

[3] Saha, N., Keskinbora, K., Suvaci, E. & Basu, B., Sintering, microstructure, mechanical, and antimicrobial properties of HAp-ZnO biocomposites, *J Biomed Mater Res B Appl Biomater*, **95**(2), pp. 430-440, 2010.

[4] Sinulingga, K., Sirait, M., Siregar, N. & Abdullah, H., Synthesis and Characterizations of Natural Limestone-Derived Nano-Hydroxyapatite (HAp): A Comparison Study of Different Metals Doped HAps on Antibacterial Activity, *RSC Adv.*, **11**(26), pp. 15896-15904, 2021.

[5] Sawai, J., Quantitative Evaluation of Antibacterial Activities of Metallic Oxide Powders (ZnO, MgO and CaO) by Conductimetric Assay, *J Microbiol Methods*, **54**(2), pp. 177-182, 2003.

[6] Zhang, L., Jiang, Y., Ding, Y., Povey, M. & York, D., Investigation into the Antibacterial Behaviour of Suspensions of ZnO Nanoparticles (ZnO Nanofluids), *Journal of Nanoparticle Research*, **9**(3), pp. 47-489, 2007.

[7] Buzuayehu, A., Amare, Z.E., Aschalew, T. & Ananda, M.H., A Review on Enhancing the Antibacterial Activity of ZnO: Mechanisms and Microscopic Investigation, *Nanoscale Res Lett.*, **15**(1), pp. 1-19, 2020.

[8] Aziz, M., Batu Kapur dan Peningkatan Nilai Tambah, *Jurnal Teknologi Mineral dan Batubara*, **6**(3), pp. 116-131, 2010.

[9] Chavali, M.S. & Nikolova, M.P., Metal Oxide Nanoparticles and Their Applications in Nanotechnology., *SN Appl Sci*., **1**(6), pp. 1-30, 2019.

[10] Koupaei, M.H., Shareghi, B., Saboury, A.A., Davar, F., Semnani, A. & Evini, M., Green Synthesis of Zinc Oxide Nanoparticles and Their Effect on the Stability and Activity of Proteinase K., *RSC Adv.,* **6**(48), pp. 42313-42323, 2016.

[11] Baladi, M., Amiri, M., Mohammadi, P., Salih Mahdi, K., Golshani, Z., Razavi, R., et al., Green Sol–Gel Synthesis of Hydroxyapatite Nanoparticles Using Lemon Extract As Capping Agent and Investigation of Its Anticancer Activity Against Human Cancer Cell Lines (T98 and SHSY5), *Arabian Journal of Chemistry*, **16**(4), pp. 1-12, 2023.

[12] Jebali, M., Colangelo, G. & Gómez-Merino, AI., Green Synthesis, Characterization, and Empirical Thermal Conductivity Assessment of ZnO Nanofluids for High-Efficiency Heat-Transfer Applications, *Materials*, **16**(4), pp. 1-17, 2023.

[13] Noviyanti, A.R., Akbar, N., Deawati, Y., Ernawati, E.E., Malik, Y.T., Fauzia, R.P., et al., A Novel Hydrothermal Synthesis Of Nanohydroxyapatite from Eggshell-Calcium-Oxide Precursors, *Heliyon*, **6**(4), e03655, 2020.

[14] Nakilcioğlu-Taş, E. & Ötleş, S., Kinetic Modelling Of Vitamin C Losses In Fresh Citrus Juices Under Different Storage Conditions, *An Acad Bras Cienc.*, **92**(2), pp. 1-9, 2020.

[15] Afifah, F. & Cahyaningrum, S.E., Sintesis dan Karakterisasi Hidroksiapatit dari Tulang Sapi (*Bos taurus*) Menggunakan Teknik Kalsinasi, *UNESA Journal of Chemistry*, **9**(3), pp. 189-196, 2020.

[16] Sharmila, G., Thirumarimurugan, M., & Muthukumaran, C., Green Synthesis of ZnO Nanoparticles Using Tecoma Castanifolia Leaf Extract: Characterization and Evaluation of Its Antioxidant, Bactericidal and Anticancer Activities, *Microchemical Journal*, **145**(3), pp. 578-587, 2019.

[17] Shabaani, M., Rahaiee, S., Zare, M. & Jafari, S.M., Green Synthesis of ZnO Nanoparticles Using Loquat Seed Extract; Biological Functions and Photocatalytic Degradation Properties, *Lwt*, **134**(4), 110133, 2020.

[18] Windarti, T., Darmawan, A. & Marliana, A., Synthesis of β-TCP by Sol-Gel Method: Variation of Ca/P Molar Ratio, *IOP Conf Ser Mater Sci Eng*., **509**(1), 012147, 2019.

[19] Bulina, N.V., Makarova, S.V., Baev, S.G., Matvienko, A.A., Gerasimov, K.B., Logutenko, O.A., et al., A Study of Thermal Stability of Hydroxyapatite, *Minerals*, **11**(12), pp. 1-15, 2021.

[20] Rial, R., González-durruthy, M., Liu, Z., & Ruso, J.M., Advanced Materials Based on Nanosized Hydroxyapatite, *Molecules*, **26**(11), pp. 1-22, 2021.

[21] Aubry, C., Drouet, C., Azaïs, T., Kim, H.J., Oh, J.M., Karacan, I., et al., Bio-Activation of HA/β-TCP Porous Scaffolds by High-Pressure CO_2 Surface Remodeling: A Novel "Coating-from" Approach, *Materials*, **15**(20), pp. 1-20, 2022.

[22 Blount, Z.D., The Unexhausted Potential of E. coli., *Elife*, **2015**(4), pp. 1-12, 2015.

[23] El-Bassyouni, G.T., Kenawy, S.H., El-Aty, A.A.A., Hamzawy, E.M.A. & Turky, G.M., Influence of ZnO Doped into Hydroxyapatite: Structural, Electrical, Biocompatibility, and Antimicrobial Assessment, *J Mol Struct*, **1268**(11), 133700, 2022.

[24] Stanić, V., Dimitrijević, S., Antić-Stanković, J., Mitrić, M., Jokić, B., Plećaš, I.B., et al., Synthesis, Characterization and Antimicrobial Activity of Copper and Zinc-Doped Hydroxyapatite Nanopowders, *Appl Surf Sci*., **256**(20), pp. 6083-60899, 2010.